



Article

# ZrB<sub>2</sub>/SiCN Thin-Film Strain Gauges for In-Situ Strain Detection of Hot Components

Fan Lin <sup>†</sup>, Xiaochuan Pan <sup>†</sup>, Chao Wu, Yingjun Zeng, Guochun Chen, Qinnan Chen <sup>\*</sup>, Daoheng Sun <sup>\*</sup> and Zhenyin Hai <sup>\*</sup>

Department of Mechanical and Electrical Engineering, School of Aerospace Engineering, Xiamen University, Xiamen 361005, China

\* Correspondence: chenqinnan@xmu.edu.cn (Q.C.); sundh@xmu.edu.cn (D.S.); haizhenyin@xmu.edu.cn (Z.H.)

† These authors contributed equally to this work.

**Abstract:** The in-situ strain/stress detection of hot components in harsh environments remains a challenging task. In this study, ZrB<sub>2</sub>/SiCN thin-film strain gauges were fabricated on alumina substrates by direct writing. The effects of ZrB<sub>2</sub> content on the electrical conductivity and strain sensitivity of ZrB<sub>2</sub>/SiCN composites were investigated, and based on these, thin film strain gauges with high electrical conductivity (1.71 S/cm) and a gauge factor of 4.8 were prepared. ZrB<sub>2</sub>/SiCN thin-film strain gauges exhibit excellent static, cyclic strain responses and resistance stability at room temperature. In order to verify the high temperature performance of the ZrB<sub>2</sub>/SiCN thin-film strain gauges, the temperature-resistance characteristic curves test, high temperature resistance stability test and cyclic strain test were conducted from 25 °C to 600 °C. ZrB<sub>2</sub>/SiCN thin-film strain gauges exhibit good resistance repeatability and stability, and highly sensitive strain response, from 25 °C to 600 °C. Therefore, ZrB<sub>2</sub>/SiCN thin-film strain gauges provide an effective approach for the measurement of in-situ strain of hot components in harsh environments.



**Citation:** Lin, F.; Pan, X.; Wu, C.; Zeng, Y.; Chen, G.; Chen, Q.; Sun, D.; Hai, Z. ZrB<sub>2</sub>/SiCN Thin-Film Strain Gauges for In-Situ Strain Detection of Hot Components. *Micromachines* **2022**, *13*, 1467. <https://doi.org/10.3390/mi13091467>

Academic Editors: Libo Gao and Zhuoqing Yang

Received: 10 August 2022

Accepted: 27 August 2022

Published: 4 September 2022

**Publisher's Note:** MDPI stays neutral with regard to jurisdictional claims in published maps and institutional affiliations.



**Copyright:** © 2022 by the authors. Licensee MDPI, Basel, Switzerland. This article is an open access article distributed under the terms and conditions of the Creative Commons Attribution (CC BY) license (<https://creativecommons.org/licenses/by/4.0/>).

**Keywords:** thin film strain gauge; direct ink writing; polymer-derived ceramics; conductive composites; high temperature

## 1. Introduction

Thin film strain gauges (TFSGs) are widely used for in-situ strain detection of various components and structures in the aerospace, transportation and automobile industries, civil engineering and even the medical field due to their advantages of non-interference, small size, fast response and in-situ integration [1–7]. TFSGs are mainly fabricated by depositing alloy/metal films such as NiCr, PdCr and TaN-Cu on the surface of components [1,8,9]. An effective TFSG must exhibit a number of appropriate properties (e.g., adequate operating range, reasonable conductivity, lack of frequency dependence), probably the most important property being the sensitivity or gauge factor (GF) [10]. However, the gauge factor (GF) of traditional metal/alloy iso piezoresistive materials is about two, resulting in low sensitivity and difficulty in detecting tiny strains.

To solve this issue, many researchers have turned to conductive composites. Conductive composites contain an insulating matrix and conductive nanoparticles dispersed therein, and the conduction mechanism and the strain sensitivity are primarily dominated by the tunneling effect [10,11]. Flexible sensors based on conductive polymer composites have stretchability and strain factors that far surpass foil strain gauges, and are widely used in wearable devices, electronic skins and human motion detection, etc. [12–17]. However, most TFSGs based on conductive composites are limited to room temperature. They are not thermally stable at high temperatures.

To construct thermally stable conductive composites with a highly sensitive piezoresistive response, the high-temperature thermal stability of the insulating matrix and the conductive phase is the first design principle. Compared to metallic and polymeric materials,

most ceramics, such as polymer-derived ceramics (PDCs) pyrolyzed at high temperature are electrically insulating and thermally stable at high temperatures [18]. Existing PDCs high temperature sensors such as temperature sensors and pressure sensors are still dominated by discrete bulk devices [19–21]. Compared with larger discrete devices, in-situ integrated TFSGs with a thickness of micrometers exhibit reproducible faster response [22]. However, the huge volume shrinkage during the pyrolysis of PDCs will cause stress mismatch at the interface of the film, leading to cracking or peeling off [23]. The use of particle fillers such as SiC, ZrO<sub>2</sub> and TiB<sub>2</sub> can not only reduce the shrinkage of the PDCs during the pyrolysis process, but also modify the properties of PDCs, such as electrical properties and mechanical properties [24]. Boride ceramics are excellent conductors of electricity with good mechanical properties, and oxidation resistance [25,26]. This makes boride ceramics promising for high temperature sensors and electrical functional devices [2,27].

In this study, PDC-SiCN was used as the insulating matrix, and the dispersed ZrB<sub>2</sub> conductive particles acted as the conductive phase. TFSG based on ceramic conductive composites was fabricated by the direct ink writing (DIW) technique based on the Weissenberg effect. Herein, the morphologies and microstructure of the ZrB<sub>2</sub>/SiCN TFSGs were characterized. The effects of ZrB<sub>2</sub> content amount on the electrical conductivity and GF of ZrB<sub>2</sub>/SiCN films were investigated. The piezoresistive response of ZrB<sub>2</sub>/SiCN TFSGs at room temperature was tested. Ultimately, high temperature performance of the ZrB<sub>2</sub>/SiCN TFSG was investigated from 25 °C to 600 °C.

## 2. Materials and Methods

### 2.1. Materials and Preparation Process

As shown in Figure 1a, commercially available PSN2 (Chinese Academy of Sciences, China) filled with ZrB<sub>2</sub> nanopowder (average diameter: 50 nm, Shanghai Chaowei Nano Technology Co., Ltd., Shanghai, China) was utilized as printing ink. The filling weight percent of ZrB<sub>2</sub> nanopowder is 40~60 wt%. The ZrB<sub>2</sub> nanopowder were uniformly dispersed in PSN2 by magnetic stirring for more than 2 h. Briefly, as shown in Figure 1b, the ink was printed by a Weissenberg-based DIW platform, which consisted of three key components: an x-y high-precision moving platform, a homemade printing setup including a printing head and a charged-coupled device camera. The printing head consists of micron tube and microneedle. The solution is quickly transported to the printing needle through the micron tube under the high-speed rotation of the microneedles. Then, the prepared thin-film strain grids were pyrolyzed in a tube furnace under nitrogen atmosphere (−0.1 MPa is evacuated before introducing nitrogen) at 800 °C for 4 h (heating rate 2 °C/min and cooling rate 3 °C/min). Finally, Ag paste was used to prepare solder joints to connect the thin-film strain grids and the Pt leads.

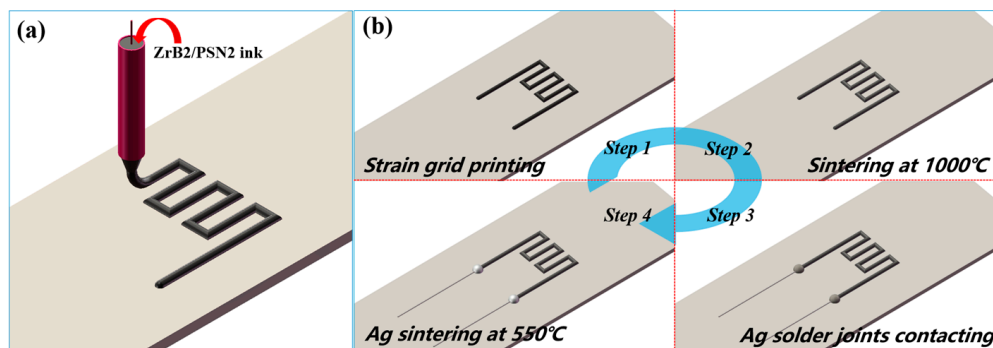


**Figure 1.** (a) Direct ink writing patterning of the strain gauge; (b) Schematic of the ZrB<sub>2</sub>/SiCN thin-film strain gauge fabrication process.

### 2.2. Experiment Setup

Strain grid thicknesses were determined by a profilometer (Dektak XT, BRUKER, Billerica, MA, USA). SEM (SUPRA55 SAPPHIRE, CARL ZEISS, Oberkochen, Battenburg,

Germany) coupled with EDS was used to characterize the morphology of the obtained samples. High temperature furnace (GSL-1700X, HF. Kejing, Hefei, China) was used to pyrolysis and high temperature furnace (OTF-1200X, HF. Kejing, Hefei, China) was used to test in high temperature.

A cantilever beam arrangement was used to investigate the strain response behavior of the  $\text{ZrB}_2/\text{SiCN}$  TFSGs, as shown in Figure 2a. One end of the beam was clamped, and the sensor was subjected to strain by applying displacement at the free end of the cantilever [2]. The corresponding resistance changes of the TFSG were recorded using data acquisition equipment. Calculate the strain at the location of the strain gauge according to the following Equation (1) [28]:

$$\varepsilon = \frac{3yhx}{2l^3} \quad (1)$$

where  $\varepsilon$  is the strain at the location of the TFSGs,  $y$  is the deflection at the free end,  $l$  is the length of the cantilever beam,  $x$  is the distance from center of strain gauge to the point of application of load and  $h$  is the thickness of the beam. The indicator for strain sensitivity of the strain gauge is defined as:

$$GF = \frac{\Delta R / R_0}{\varepsilon} \quad (2)$$

where  $\Delta R$  is the change of TFSG resistance when strain  $\varepsilon$  is applied and  $R_0$  is the initial resistance of TFSG. The piezoresistive response of TFSG at high temperatures was done in a high temperature furnace. The tube furnace is heated to  $600\text{ }^\circ\text{C}$  at  $12\text{ }^\circ\text{C}/\text{min}$ . In the meantime, the stepper motor is applied strain to the free end of the cantilever beam to obtain the strain response at high temperatures.

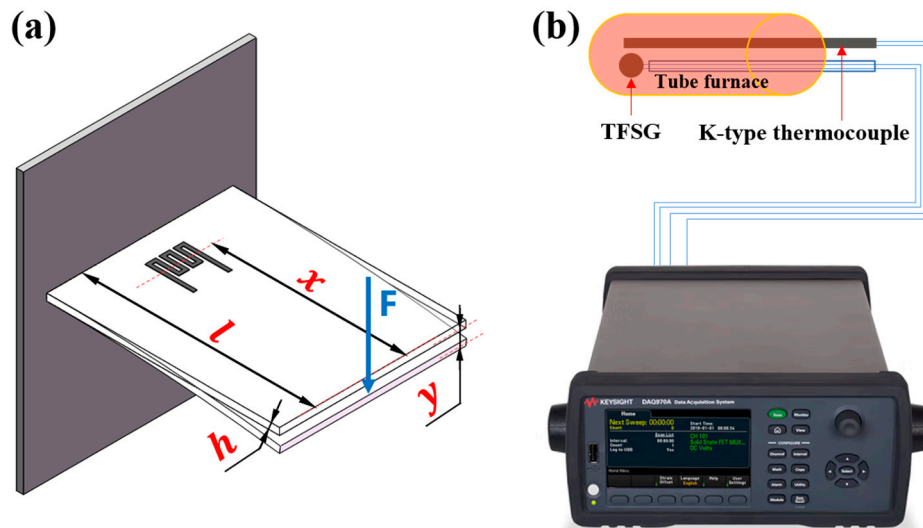


**Figure 2.** Schematic of experiment setups for (a) strain response testing and (b) temperature resistance characteristics testing.

The high temperature resistance test system of the strain gauge is shown in Figure 2b, which consists of a tube furnace and a standard k-type thermocouple. The unit of TCR is  $\text{ppm}/\text{ }^\circ\text{C}$  and is used to express the relationship between the resistance of the strain gauge and the temperature. TCR can be calculated by the following Equation (3) [29]:

$$\text{TCR} = \frac{dR}{RdT} \times 10^6 \quad (3)$$

### 3. Results

#### 3.1. Microstructural Characterisation of $\text{ZrB}_2/\text{SiCN}$ TFSG

The fabricated  $\text{ZrB}_2/\text{SiCN}$  TFSGs on  $\text{Al}_2\text{O}_3$  substrate are shown in Figure 3a. The length and width of  $\text{ZrB}_2/\text{SiCN}$  TFSGs are 7 mm and 5 mm, respectively. Its line width and

thickness were determined by the profilometer, and were 600  $\mu\text{m}$  and 15  $\mu\text{m}$ , respectively. Porosity, cracks and inhomogeneity are the main factors affecting the electrical conductivity and thermal stability of TFSG. The low-magnification SEM image of  $\text{ZrB}_2/\text{SiCN}$  TFSGs is shown in Figure 3c. There are no obvious cracks on the surface of  $\text{ZrB}_2/\text{SiCN}$  TFSGs. The high-magnification SEM image of  $\text{ZrB}_2/\text{SiCN}$  TFSGs in Figure 3d shows a dense and crack-free surface. The SEM cross-sectional image presented in Figure 3e shows that the interface is clearly visible, and the sensitive grid is tightly bonded to the substrate without an obvious gap.

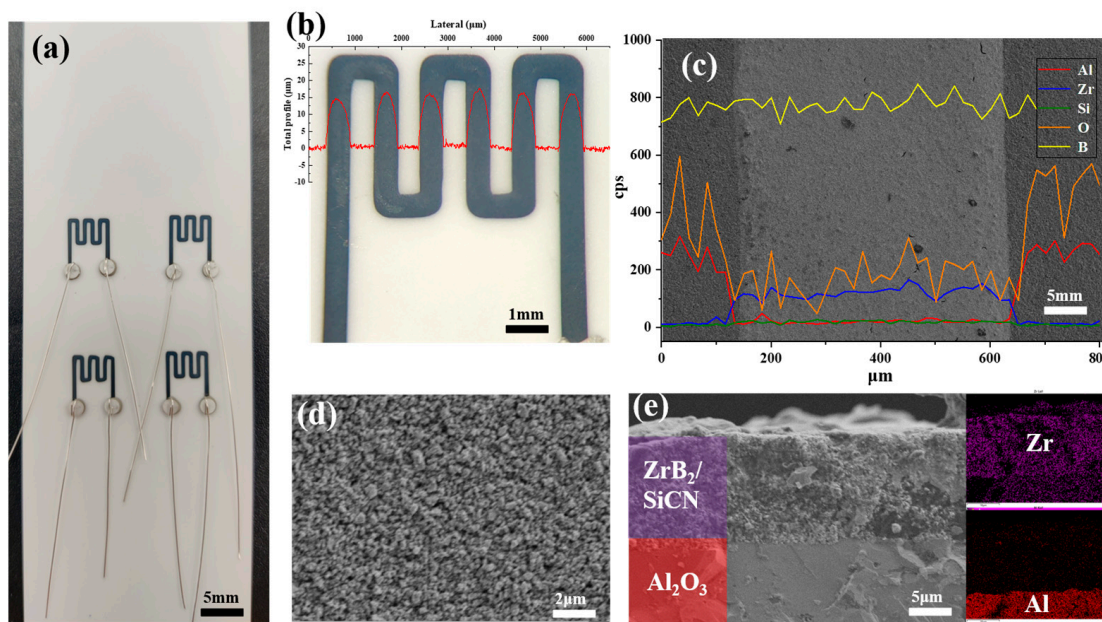


**Figure 3.** (a) Samples of the thin film strain gauge; (b) Thickness and width of strain grids; (c) Low-magnification SEM image and EDS analysis of TFSGs; (d) High-magnification SEM image of TFSGs; (e) The cross-sectional SEM images and EDS analysis of TFSGs.

### 3.2. Piezoresistive Response of $\text{ZrB}_2/\text{SiCN}$ TFSG

The electrical conductivities of the printed  $\text{ZrB}_2(40 \text{ wt\%})/\text{SiCN}$ ,  $\text{ZrB}_2(50 \text{ wt\%})/\text{SiCN}$ ,  $\text{ZrB}_2(60 \text{ wt\%})/\text{SiCN}$  strained grids are 0.036 S/cm, 0.077 S/cm and 1.71 S/cm, respectively. With the increase of  $\text{ZrB}_2$  nanopowder filling, the electrical conductivity of the strain grids increases significantly, which is related to the conductive network composed of  $\text{ZrB}_2$  in  $\text{ZrB}_2/\text{SiCN}$  composites. To investigate the piezoresistive behavior of  $\text{ZrB}_2/\text{SiCN}$  TFSGs in detail, their strain responses were tested using the deflection method at room temperature. The strain responses of the  $\text{ZrB}_2(40 \text{ wt\%})/\text{SiCN}$  TFSG at room temperature are shown in Figure 4a–d. Figure 4a shows the static strain response of the  $\text{ZrB}_2(40 \text{ wt\%})/\text{SiCN}$  TFSG. Strain was applied sequentially in 100  $\mu\epsilon$  increments, and the change in resistance was consistent with the strain applied to the sensor as time progresses. The  $\text{ZrB}_2(40 \text{ wt\%})/\text{SiCN}$  TFSG exhibits a good response that stepwise applied strain leads to a distinguishable, recoverable step change in the resistance of the TFSG. The  $\text{ZrB}_2(40 \text{ wt\%})/\text{SiCN}$  TFSG exhibits a positive GF, that is, the resistance increases with increasing positive strain and decreases with increasing negative strain. Figure 4b shows the strain responses of  $\text{ZrB}_2(40 \text{ wt\%})/\text{SiCN}$  TFSG under different strain amounts, where strains of 100  $\mu\epsilon$ , 200  $\mu\epsilon$ , 300  $\mu\epsilon$ , 400  $\mu\epsilon$ , and 500  $\mu\epsilon$  were sequentially applied to the TFSG at a constant strain rate of 100  $\mu\epsilon/\text{s}$ . Figure 4c,d show the strain response of 500  $\mu\epsilon$  at different strain rates (20  $\mu\epsilon/\text{s}$ , 50  $\mu\epsilon/\text{s}$ , 100  $\mu\epsilon/\text{s}$ , 200  $\mu\epsilon/\text{s}$ , and 400  $\mu\epsilon/\text{s}$ ) and the cyclic strain response with a period of 4 s, respectively. The applied strains were all 500  $\mu\epsilon$ . Consistent changes in relative resistance indicate that the  $\text{ZrB}_2(40 \text{ wt\%})/\text{SiCN}$  TFSG has a stable and strain-rate independent strain response.

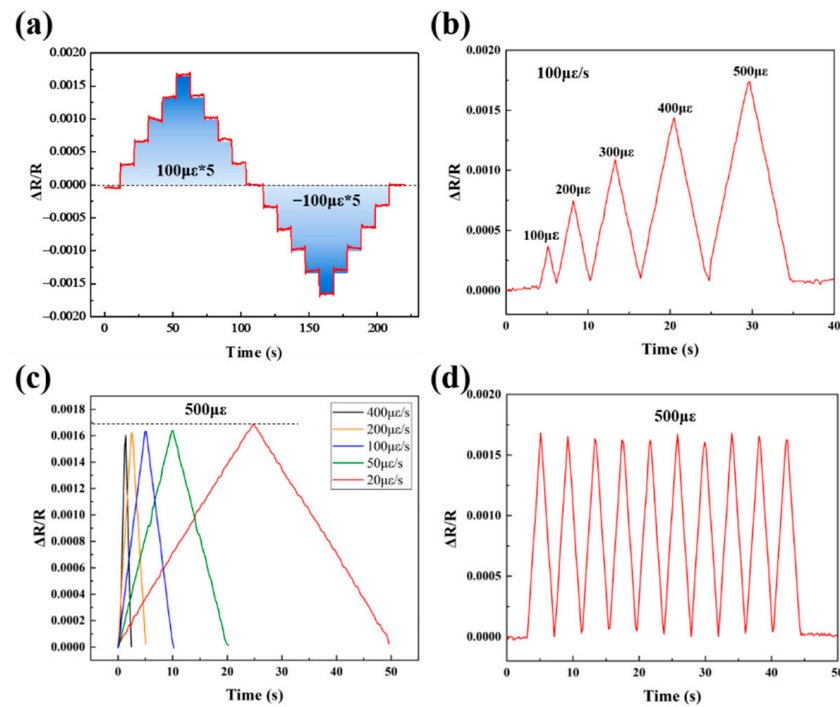


**Figure 4.** Piezoresistive response of the ZrB<sub>2</sub>(40 wt%)/SiCN TFSG: (a) The static response; (b) The response of different strain quantities at a constant strain rate ( $100 \mu\epsilon/s$ ); (c) The response at different strain rates; (d) The cyclic response.

The strain responses of ZrB<sub>2</sub>(50 wt%)/SiCN TFSG at room temperature are shown in Figure 5a–d. Similar to ZrB<sub>2</sub>(40 wt%)/SiCN TFSG, ZrB<sub>2</sub>(50 wt%)/SiCN TFSG exhibits stable, distinguishable strain responses.

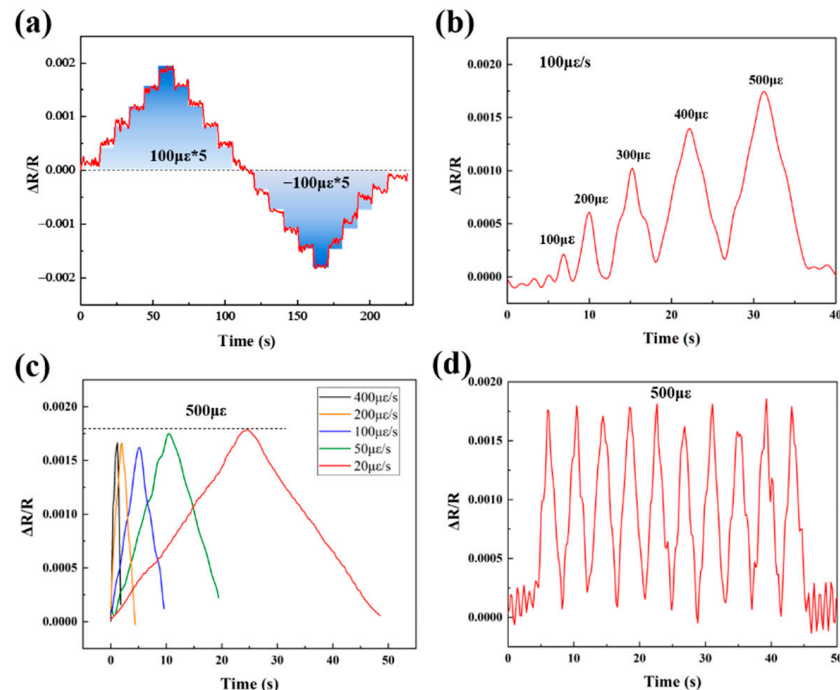


**Figure 5.** Piezoresistive response of the ZrB<sub>2</sub>(50 wt%)/SiCN TFSG: (a) The static response; (b) The response of different strain quantities at a constant strain rate ( $100 \mu\epsilon/s$ ); (c) The response at different strain rates; (d) The cyclic response.

The strain responses of ZrB<sub>2</sub>(60 wt%)/SiCN TFSG at room temperature are shown in Figure 6a–d. Compared with ZrB<sub>2</sub>(40 wt%)/SiCN and ZrB<sub>2</sub>(50 wt%)/SiCN TFSGs, the strain signal of ZrB<sub>2</sub>(60 wt%)/SiCN TFSG is more obvious.

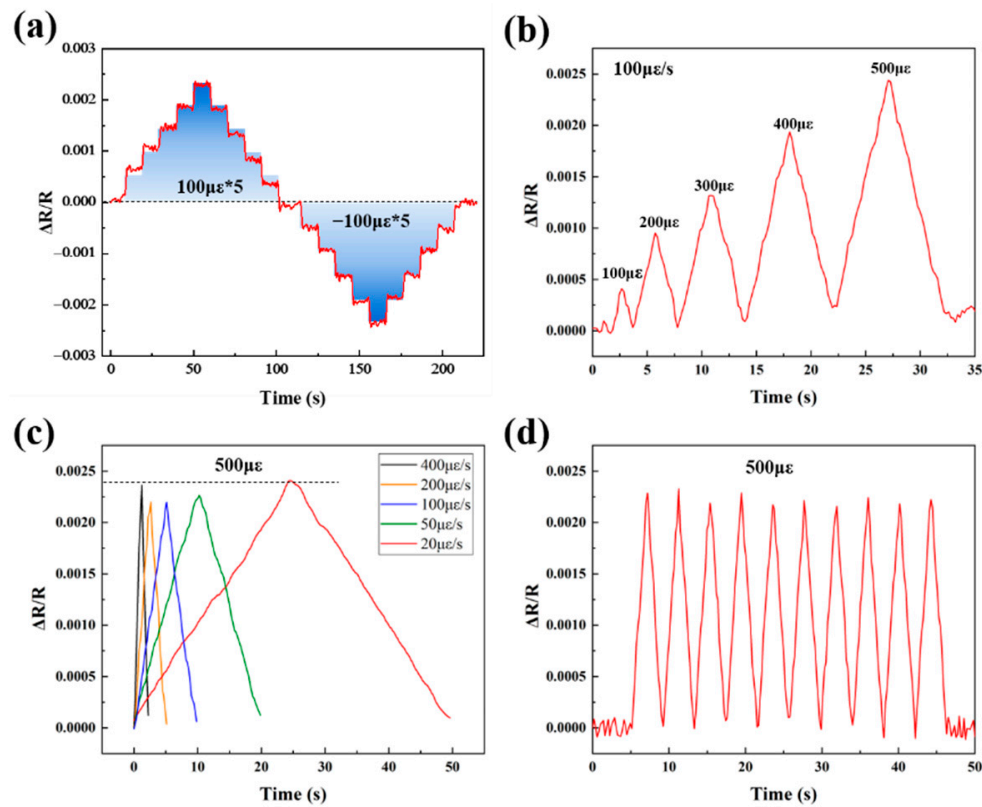


**Figure 6.** Piezoresistive response of the ZrB<sub>2</sub>(60 wt%)/SiCN TFSG: (a) The static response; (b) The response of different strain quantities at a constant strain rate ( $100 \mu\epsilon/s$ ); (c) The response at different strain rates; (d) The cyclic response.

The GFs of the ZrB<sub>2</sub>/SiCN TFSGs were calculated according to Equation (2). The GFs of ZrB<sub>2</sub>(40 wt%)/SiCN, ZrB<sub>2</sub>(50 wt%)/SiCN and ZrB<sub>2</sub>(60 wt%)/SiCN at room temperature are 3.4, 3.3 and 4.8, respectively (see Figure 7). Comparing the GF of TFSG with different ZrB<sub>2</sub> filling amount, the GF of ZrB<sub>2</sub>(60 wt%)/SiCN is the highest, which is mainly owing to the change in resistivity by the concentration of ZrB<sub>2</sub> conductive phase, which leads to the increase of the effect of piezoresistive response. Guenter Schultes et al. fabricated boride TFSG on a Al<sub>2</sub>O<sub>3</sub> substrate by DC magnetron sputtering and obtained 0.7 GF [26]. In contrast, the GF of TFSG based on ZrB<sub>2</sub>/SiCN conductive ceramic composite is several times higher than that of single boride TFSG.

### 3.3. High Temperature Performance of the ZrB<sub>2</sub>/SiCN TFSG

Since ZrB<sub>2</sub>(60 wt%)/SiCN TFSG exhibited higher conductivity and strain sensitivity, its high temperature performance was tested. In practical applications, the consistency of the temperature-resistance characteristics during the cycle temperature and high temperature resistance stability of the TFSG are very important, and it reflects the stability and oxidation resistance of the TFSG at high temperatures. In order to study the repeatability of the temperature resistance of ZrB<sub>2</sub>(60 wt%)/SiCN TFSG, we tested the temperature-resistance characteristic curves of two times of heating and cooling (Figure 8a). ZrB<sub>2</sub>(60 wt%)/SiCN TFSG exhibited a negative temperature coefficient of resistance of  $-428 \text{ ppm}/^\circ\text{C}$  and good repeatability in the range of 25–600  $^\circ\text{C}$ . Figure 8b shows the resistance change curves of ZrB<sub>2</sub>(60 wt%)/SiCN TFSG at 600  $^\circ\text{C}$  for 2 h. ZrB<sub>2</sub>(60 wt%)/SiCN TFSG exhibited excellent resistance stability and antioxidant qualities at 600  $^\circ\text{C}$ , and resistance increased by 1.3% after two hours of oxidation. The good repeatability, stability and consistency of the resistance

of ZrB<sub>2</sub>(60 wt%)/SiCN TFSG are attributed to the oxide layer formed on the surface of the film, which prevents the further diffusion of oxygen [30].

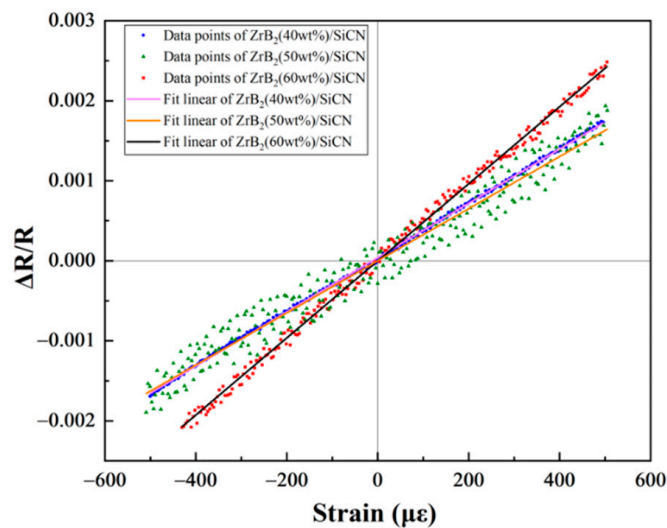


**Figure 7.** The GFs of the ZrB<sub>2</sub>/SiCN TFSGs.

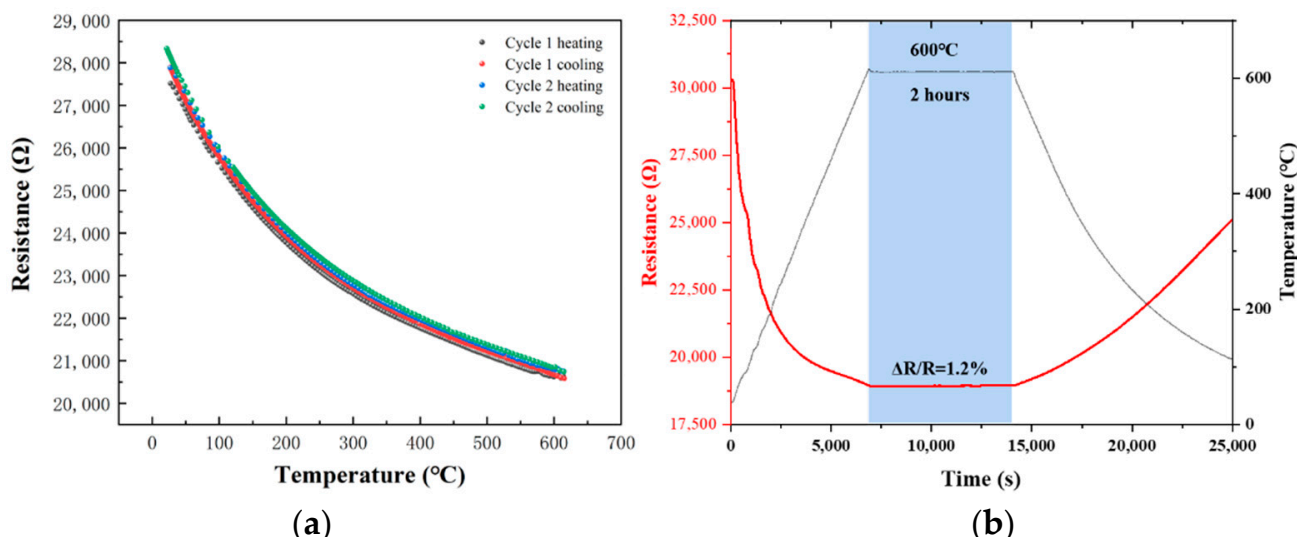


**Figure 8.** (a) R-T curves of ZrB<sub>2</sub>(60 wt%)/SiCN TFSG from room temperature to 600 °C; (b) Resistance change curves of ZrB<sub>2</sub>(60 wt%)/SiCN TFSG at 600 °C for 2 h.

To evaluate the strain response of ZrB<sub>2</sub>(60 wt%)/SiCN TFSG at high temperatures, cyclic strain tests were carried out from room temperature to 600 °C, as shown in Figure 9a. The curves of the cyclic strain response were intercepted at 400 °C, 500 °C and 600 °C, respectively, as shown in the Figure 9b–d. ZrB<sub>2</sub>(60 wt%)/SiCN TFSG exhibits good repeatability and stability resistance at high temperatures. Although the overall resistance decreases with increasing temperature due to the temperature-resistance effect, the pulse signal caused by the cyclic strain is clearly visible. The above high-temperature test results show that ZrB<sub>2</sub>(60 wt%)/SiCN TFSG has good resistance stability and highly sensitive strain response in the temperature range from room temperature to 600 °C, and has potential application in the field of hot component strain monitoring/sensing.

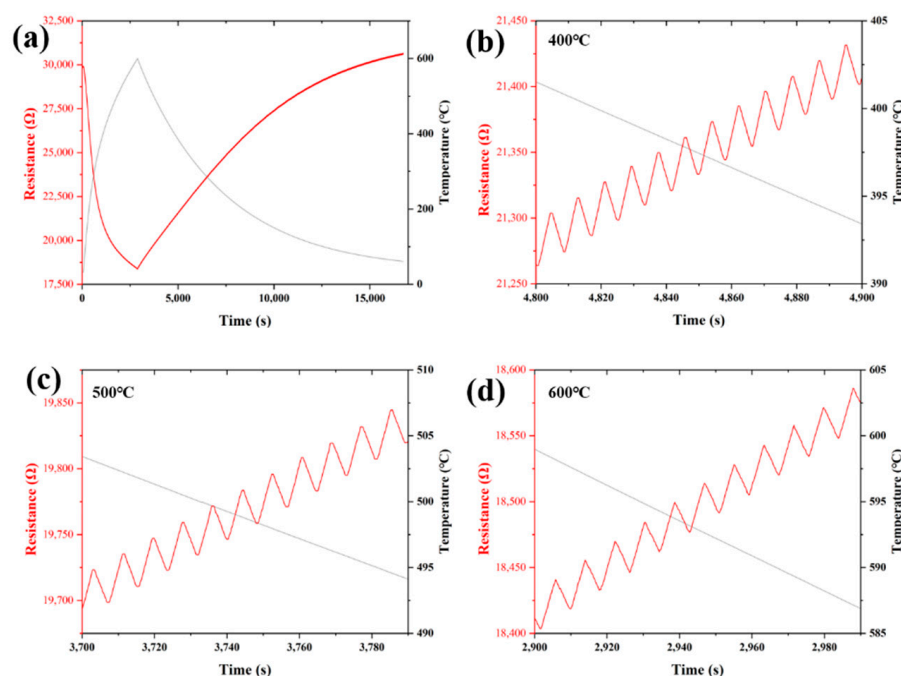


**Figure 9.** (a) The cyclic response from 25  $^{\circ}\text{C}$  to 600  $^{\circ}\text{C}$ ; (b) The cyclic response at 400  $^{\circ}\text{C}$ ; (c) The cyclic response at 500  $^{\circ}\text{C}$ ; (d) The cyclic response at 600  $^{\circ}\text{C}$ .

#### 4. Discussion

$\text{ZrB}_2/\text{SiCN}$  TFSGs were fabricated on alumina substrates by DIW of the Weissenberg effect. The used DIW process enabled thin-film patterning and in situ strain/stress sensing of high-temperature components. The  $\text{ZrB}_2/\text{SiCN}$  TFSGs were characterized to determine the structural dimensions, surface topography and cross-sectional structure by SEM. The piezoresistive behavior of  $\text{ZrB}_2/\text{SiCN}$  TFSGs at room temperature was investigated by the deflection method.  $\text{ZrB}_2/\text{SiCN}$  TDGSs exhibited excellent strain responses and resistance stability at room temperature. The effects of  $\text{ZrB}_2$  content on the electrical conductivity and strain sensitivity of  $\text{ZrB}_2/\text{SiCN}$  composites were investigated. Finally,  $\text{ZrB}_2(60 \text{ wt\%})/\text{SiCN}$  film with high conductivity (1.71 S/cm) and GF of 4.8 was used as the sensitive material for high-temperature thin-film strain gauges. The temperature-resistance characteristic curves of  $\text{ZrB}_2(60 \text{ wt\%})/\text{SiCN}$  TFSGs were tested, and the TFSGs exhibited a negative temperature coefficient of resistance of  $-428 \text{ ppm}/^{\circ}\text{C}$  and good repeatability in the range of 25–600  $^{\circ}\text{C}$ . The resistance change curves of  $\text{ZrB}_2(60 \text{ wt\%})/\text{SiCN}$  TFSGs were tested at 600  $^{\circ}\text{C}$ . The TFSGs have good resistance stability with resistance increasing by 1.3% after two hours of oxidation at 600  $^{\circ}\text{C}$ . Finally, the strain response verification was conducted from 25  $^{\circ}\text{C}$  to 600  $^{\circ}\text{C}$ .  $\text{ZrB}_2(60 \text{ wt\%})/\text{SiCN}$  TFSG has a highly sensitive strain response from 25  $^{\circ}\text{C}$  to 600  $^{\circ}\text{C}$ . Therefore,  $\text{ZrB}_2/\text{SiCN}$  TFSGs based on the Weissenberg DIW can be applied to micro-strain detection from room temperature to 600  $^{\circ}\text{C}$ . Further research is underway to improve the antioxidant nature of  $\text{ZrB}_2/\text{SiCN}$  TFSGs for applying to higher temperatures.

**Author Contributions:** Conceptualization, F.L. and X.P.; methodology, F.L. and X.P.; software, F.L.; validation, C.W. and F.L.; formal analysis, X.P.; investigation, F.L.; resources, C.W.; data curation, G.C.; writing—original draft preparation, F.L.; writing—review and editing, Z.H.; visualization, F.L. and Y.Z.; supervision, Z.H.; project administration, Q.C.; funding acquisition, D.S. All authors have read and agreed to the published version of the manuscript.

**Funding:** This research was funded by China Aviation Research Institute, Shenyang Engine Design and Research Institute (Grant number JC3602007026).

**Institutional Review Board Statement:** Not applicable.

**Informed Consent Statement:** Not applicable.

**Data Availability Statement:** Not applicable.

**Conflicts of Interest:** The authors declare no conflict of interest.

## References

1. Liu, H.; Mao, X.L.; Yang, Z.B.; Cui, J.T.; Jiang, S.W.; Zhang, W.L. High temperature static and dynamic strain response of PdCr thin film strain gauge prepared on Ni-based superalloy. *Sens. Actuators A Phys.* **2019**, *298*, 111571. [[CrossRef](#)]
2. Wu, C.; Pan, X.C.; Lin, F.; Cui, Z.F.; He, Y.P.; Chen, G.C.; Zeng, Y.J.; Liu, X.L.; Chen, Q.N.; Sun, D.H.; et al. TiB<sub>2</sub>/SiCN Thin-Film Strain Gauges Fabricated by Direct Writing for High-Temperature Application. *IEEE Sens. J.* **2022**, *22*, 11517–11525. [[CrossRef](#)]
3. Ayerdi, I.; Castano, E.; Garciaalonso, A.; Gracia, F.J. Characterization of tantalum oxynitride thin-films as high-temperature strain-gauges. *Sens. Actuators A Phys.* **1995**, *46*, 218–221. [[CrossRef](#)]
4. Yang, S.Y.; Zhang, C.C.; Yang, Z.Q.; Wang, H.; Zhao, X.L.; Ding, G.F. In-situ self-compensated pt-ito thin film strain gage with a nanolaminated structure. In Proceedings of the 20th International Conference on Solid-State Sensors, Actuators and Microsystems and Eurosensors XXXIII (TRANSDUCERS and EUROSENSORS), Berlin, Germany, 23–27 June 2019; pp. 2005–2008.
5. Gregory, O.J.; Luo, Q.; Crisman, E.E. High temperature stability of indium tin oxide thin films. *Thin Solid Films* **2002**, *406*, 286–293. [[CrossRef](#)]
6. Chung, G.S. Characteristics of tantalum nitride thin film strain gauges for harsh environments. *Sens. Actuators A Phys.* **2007**, *135*, 355–359. [[CrossRef](#)]
7. Fiorillo, A.S.; Critello, C.D.; Pullano, S.A. Theory, technology and applications of piezoresistive sensors: A review. *Sens. Actuators A Phys.* **2018**, *281*, 156–175. [[CrossRef](#)]
8. Wang, H.Y.; Liu, K.; An, Z.H.; Wu, X.; Huang, X. Ion-Beam Sputtered Thin-Film Strain-Gauge Pressure Transducers. *Sens. Actuators A Phys.* **1993**, *35*, 265–268.
9. Wang, C.M.; Hsieh, J.H.; Li, C. Electrical and piezoresistive properties of TaN-Cu nanocomposite thin films. *Thin Solid Films* **2004**, *469*, 455–459. [[CrossRef](#)]
10. Garcia, J.R.; O'Suilleabhain, D.; Kaur, H.; Coleman, J.N. A Simple Model Relating Gauge Factor to Filler Loading in Nanocomposite Strain Sensors. *ACS Appl. Nano Mater.* **2021**, *4*, 2876–2886. [[CrossRef](#)]
11. Sanli, A.; Benchirouf, A.; Muller, C.; Kanoun, O. Piezoresistive performance characterization of strain sensitive multi-walled carbon nanotube-epoxy nanocomposites. *Sens. Actuators A Phys.* **2017**, *254*, 61–68. [[CrossRef](#)]
12. Boland, C.S.; Khan, U.; Ryan, G.; Barwick, S.; Charifou, R.; Harvey, A.; Backes, C.; Li, Z.; Ferreira, M.S.; Mobius, M.E.; et al. Sensitive electromechanical sensors using viscoelastic graphene-polymer nanocomposites. *Science* **2016**, *354*, 1257–1260. [[CrossRef](#)] [[PubMed](#)]
13. Wu, Y.T.; Yan, T.; Zhang, K.Q.; Pan, Z.J. A Hollow Core-Sheath Composite Fiber Based on Polyaniline/Polyurethane: Preparation, Properties, and Multi-Model Strain Sensing Performance. *Adv. Mater. Technol.* **2022**, *2200777*. [[CrossRef](#)]
14. Lin, Y.K.; Yin, Q.; Wang, J.; Jia, H.B.; Yuan, G.L.; Wang, J.Y. Sensitivity enhanced, highly stretchable, and mechanically robust strain sensors based on reduced graphene oxide-aramid nanofibers hybrid fillers. *Chem. Eng. J.* **2022**, *443*, 136468. [[CrossRef](#)]
15. Rinaldi, A.; Tamburrano, A.; Fortunato, M.; Sarto, M.S. A Flexible and Highly Sensitive Pressure Sensor Based on a PDMS Foam Coated with Graphene Nanoplatelets. *Sensors* **2016**, *16*, 2148. [[CrossRef](#)] [[PubMed](#)]
16. Chen, H.T.; Miao, L.M.; Su, Z.M.; Song, Y.; Han, M.D.; Chen, X.X.; Cheng, X.L.; Chen, D.M.; Zhang, H.X. Fingertip-inspired electronic skin based on triboelectric sliding sensing and porous piezoresistive pressure detection. *Nano Energy* **2017**, *40*, 65–72. [[CrossRef](#)]
17. Yamada, T.; Hayamizu, Y.; Yamamoto, Y.; Yomogida, Y.; Izadi-Najafabadi, A.; Futaba, D.N.; Hata, K. A stretchable carbon nanotube strain sensor for human-motion detection. *Nat. Nanotechnol.* **2011**, *6*, 296–301. [[CrossRef](#)]
18. Wu, C.; Pan, X.C.; Lin, F.; Cui, Z.F.; Li, X.; Chen, G.C.; Liu, X.L.; He, Y.P.; He, G.H.; Hai, Z.Y.; et al. High-temperature electrical properties of polymer-derived ceramic SiBCN thin films fabricated by direct writing. *Ceram. Int.* **2022**, *48*, 15293–15302. [[CrossRef](#)]
19. Zhang, L.G.; Wang, Y.S.; An, L.N. Piezoresistivity of polymer-derived AlSiCN ceramics. In *Applied Materials and Technologies for Modern Manufacturing, Pts 1–4*; Trans Tech Publications Ltd.: Bäch, Switzerland, 2013; Volume 423–426, pp. 89–92. [[CrossRef](#)]
20. Yu, Y.D.; Li, J.P.; Niu, J.H.; Yi, F.J.; Meng, S.H. The stability and repeatability of high temperature electrical properties of SiAlCN ceramic sensor heads. *Ceram. Int.* **2019**, *45*, 7588–7593. [[CrossRef](#)]
21. Zhao, R.; Shao, G.; Cao, Y.J.; An, L.N.; Xu, C.Y. Temperature sensor made of polymer-derived ceramics for high-temperature applications. *Sens. Actuators A Phys.* **2014**, *219*, 58–64. [[CrossRef](#)]
22. Fu, X.L.; Lin, Q.Y.; Peng, Y.Q.; Liu, J.H.; Yang, X.F.; Zhu, B.P.; Ouyang, J.; Zhang, Y.; Xu, L.C.; Chen, S. High-Temperature Heat Flux Sensor Based on Tungsten-Rhenium Thin-Film Thermocouple. *IEEE Sens. J.* **2020**, *20*, 10444–10452. [[CrossRef](#)]
23. Lu, K.; Erb, D. Polymer derived silicon oxycarbide-based coatings. *Int. Mater. Rev.* **2018**, *63*, 139–161. [[CrossRef](#)]
24. Barroso, G.; Li, Q.; Bordia, R.K.; Motz, G. Polymeric and ceramic silicon-based coatings—A review. *J. Mater. Chem. A* **2019**, *7*, 1936–1963. [[CrossRef](#)]
25. Ni, D.W.; Cheng, Y.; Zhang, J.P.; Liu, J.X.; Zou, J.; Chen, B.W.; Wu, H.Y.; Li, H.J.; Dong, S.M.; Han, J.C.; et al. Advances in ultra-high temperature ceramics, composites, and coatings. *J. Adv. Ceram.* **2022**, *11*, 1–56. [[CrossRef](#)]
26. Schultes, G.; Schmitt, M.; Goettel, D.; Freitag-Weber, O. Strain sensitivity of TiB<sub>2</sub>, TiSi<sub>2</sub>, TaSi<sub>2</sub> and WSi<sub>2</sub> thin films as possible candidates for high temperature strain gauges. *Sens. Actuators A Phys.* **2006**, *126*, 287–291. [[CrossRef](#)]

27. Wu, C.; Lin, F.; Pan, X.C.; Cui, Z.F.; He, Y.P.; Chen, G.C.; Liu, X.L.; He, G.H.; Chen, Q.N.; Sun, D.H.; et al. TiB<sub>2</sub>-Modified Polymer-Derived Ceramic SiCN Double-Layer Thin Films Fabricated by Direct Writing for High-Temperature Application. *Adv. Eng. Mater.* **2022**, *22*, 2200228. [[CrossRef](#)]
28. Ren, S.; Jiang, S.W.; Liu, H.; Zhang, W.L.; Li, Y.R. Investigation of strain gauges based on interdigitated Ba<sub>0.5</sub>Sr<sub>0.5</sub>TiO<sub>3</sub> thin film capacitors. *Sens. Actuators A Phys.* **2015**, *236*, 159–163. [[CrossRef](#)]
29. Wen, M.; Guan, X.C.; Li, H.; Ou, J.P. Temperature characteristics of thick-film resistors and its application as a strain sensor with low temperature-sensitivity. *Sens. Actuators A Phys.* **2020**, *301*, 111779. [[CrossRef](#)]
30. Parthasarathy, T.A.; Rapp, R.A.; Opeka, M.; KeranS, R.J. A model for the oxidation of ZrB<sub>2</sub>, HfB<sub>2</sub> and TiB<sub>2</sub>. *Acta Mater.* **2007**, *55*, 5999–6010. [[CrossRef](#)]